Radio Science, Volume 15, Number 4, pages 843–853, July–August 1980

Methods for the extraction of long-period ocean wave parameters from narrow beam HF radar sea echo

Belinda Lipa

SRI International, Menlo Park, California 94025

Donald Barrick

NOAA Wave Propagation Laboratory, Boulder, Colorado 80302

(Received September 21, 1979; revised February 21, 1980; accepted February 21, 1980.)

This paper describes inversion methods for HF radar sea echo Doppler spectra, giving parameters of the ocean wave spectrum in the important long-wavelength region. Radar spectra exhibiting very narrow spikes in the higher-order structure adjacent to the first-order lines are indicative of ocean wave components with a single dominant wavelength. In the simplest method of interpretation these components are assumed to be unidirectional; in this case we show how to extract wave period, direction, and rms wave height. If this simple model does not provide a good fit to the data or if the radar side bands have the form of broad peaks, we use a model for the wave spectrum with a cardioid distribution in direction and a Gaussian distribution in wave frequency. Parameters identifiable from this model include the rms wave height, dominant direction and period, and the angular spread in the direction and frequency distributions. In normal surface wave experiments the major source of error or noise is the random surface height of the sea; we describe the resulting statistics of the radar spectrum and trace the propagation of uncertainty to the derived ocean parameters.

1. INTRODUCTION

Crombie [1955] discovered the mechanism behind high-frequency (HF) radar sea scatter nearly 25 years ago by spectrally analyzing the received time series. Using the gravity wave dispersion equation that relates the velocity to the square root of the ocean wavelength, he correctly deduced that the two sharp, symmetrically positioned Doppler peaks were produced by those ocean wave trains exactly half the radio wavelength, moving toward and away from the radar. We now call these prominent peaks the 'Bragg lines,' since the mechanism producing them is the first-order Bragg effect. When theories confirmed this mechanism [*Wait,* 1966; *Barrick,* 1972] and showed that the strength of these echo peaks is proportional to the heights of the corresponding Bragg-scattering ocean wave trains, scientists became enthusiastic about the prospect of using HF radars to measure sea state parameters. In order to make direct observations of the long ocean waves that are the essence of 'sea state' using this first-order Bragg effect, one would have to operate the radar at lower MF; huge antenna size requirements, heavy spectrum utilization in this region, and ionospheric problems all dictate against such a system [*Barrick,* 1977*b*; *Barrick and Lipa,* 1979*a*]. At mid and upper HF the first-order Bragg peaks are produced by the less interesting shorter waves, and hence using these alone, radio oceanographers resigned themselves to extracting only wind direction information because the short waves align themselves quickly with the wind [*Long and Trizna,* 1973; *Stewart and Barnum,* 1975].

The more sophisticated radar systems and digital signal processors of the mid-1960's showed a lower-level spectral continuum surrounding the first-order Bragg peaks that was definitely established as sea echo. *Barrick* [1971, 1972] derived a theoretical expression for this continuum, showing that it was produced by second-order ocean wave-wave interactions. He expressed the power spectral density at each frequency as an integral over a product of two wave height directional spectra, the arguments of which were the double Bragg-interacting wave vectors, and suggested the possibility that the integral equation could be inverted to give the

This paper is not subject to U.S. copyright. Published in 1980 by the American Geophysical Union.

directional spectrum of the long ocean waves of greatest interest. This method would be both powerful and practical, involving measurements at a single HF frequency. *Hasselmann* [1971], however, observed that if the kernal of the integral (referred to as the transfer function or coupling coefficient) were a constant, the second-order spectral continuum would nearly replicate the ocean nondirectional spectrum, thereby yielding no long-wave directional information. *Barrick* [1977*a*] developed and tested an approximate technique that yielded this nondirectional information for longer waves (i.e., wave height, dominant wave period, and the nondirectional spectrum) by combining the two second-order peaks surrounding each Bragg line; indeed, the results proved to be relatively insensitive to direction. *Maresca and Georges* [1980] developed an even simpler method to obtain wave height by combining the energy in both second-order spectral side bands; again, this process renders the results insensitive to direction. All of this suggested that extracting directional information on long waves from the second-order echo might prove elusive (even though wave height and period were obtainable).

Lipa [1977, 1978] was the first to show that directional information can be derived from the second-order echo, even though she concentrated on the short-period wind wave region and used a model that separated the directional and frequency dependences as independent multiplicative factors. Often the directional dependence is dependent on wave number, as when swell components and wind waves with different wave numbers arrive from different directions; hence this model is not generally valid. An example is illustrated in the sea echo Doppler spectrum of Figure 1, where second-order wind wave and swell peaks are both present and are from different directions.

This paper shows that the direction of long-period ocean waves (as well as height and period) may indeed be derived from the second-order sea echo spectral peaks. This reversal in outlook results from closer examination of models of the radar Doppler spectrum produced by these waves, which shows that (1) the positions of the higher-order echo peaks vary slightly with wave direction and (2) the amplitudes of the echo peaks depend fairly strongly on the coupling coefficient, and this in turn is shown here to vary significantly with wave direction. Consequently, we have been able to develop analytical techniques for extracting the directional ocean wave spectrum in the long-wavelength region.

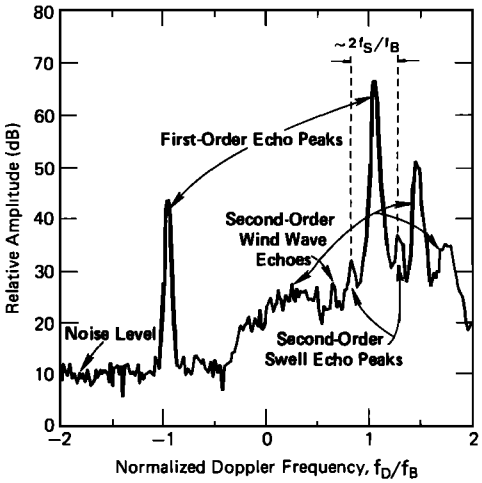

Fig. 1. Narrow beam sea echo Doppler spectrum at 9.4 MHz measured at San Clemente Island on December 4, 1972, 1114–1156. Thirteen 204.8-s spectra were averaged to produce this result, illustrating the first-order Bragg peaks, second-order swell peaks, and second-order wind wave peaks. Independent buoy observation showed 14-s swell of 0.76-m significant height, along with wind waves having 1.83-m significant height.

In this analysis we restrict consideration to ocean waves with periods greater than 10 s and to radar frequencies in the upper HF band. This allows considerable simplification of the integral equation describing the second-order Doppler spectrum, and as a result we can linearize the integral equation and in some cases employ simple models for the ocean wave spectrum. Severe storms or hurricanes will often arouse these long-period waves directly; the phase velocity of waves produced by this mechanism does not exceed the wind velocity. For example, the phase speed of waves directly excited by 20 m/s (~40 kn) winds should not exceed 12.8 s. Recent studies [*Hasselmann et al.*, 1976] show that long-period waves are also generated by energy transfer from higher-order nonlinear interactions among the shorter waves.

Oceanographers technically define swell as waves produced in another area and/or at an earlier time [*Kinsman*, 1965]. In contrast to 'wind waves' that are constantly generated by local winds, swell waves appear more organized (their quasi-sinusoidal nature permits the identification of a direction and period) and generally have longer periods. Swells with periods between 10 and 18 s are nearly always

observed on the oceans even though local winds may be quite low.

In section 2 we give the theoretical expressions for the first-order and second-order radar cross sections and describe how the second-order integral is linearized and how the data are averaged over frequency. Section 3 describes the interpretation of the radar spectra in terms of the directional ocean wave spectrum. When the higher-order spectral peaks are narrow, simple models of the ocean wave spectrum are applicable, allowing the derivation of closed-form solutions. The simplest model applies when the finite-sized storm-generating area recedes to infinity in distance and past time; in this limit the directional spectrum of the swell produced becomes an impulse function in wave frequency and direction. Such a model is usually applicable when the storm area was more than 2000 km distant from the observer and will be shown to produce a Doppler spectrum also consisting of impulse functions. When the storm-generating area is closer, the ocean waves may be spread over a narrow frequency band and also be spread in angle. In this case we use a model wave spectrum with a cardioid distribution in angle and a Gaussian distribution in wave height. This model will be shown to produce narrow peaks in the Doppler spectrum, whose width is dependent mainly on the width of the ocean wave frequency band, with energies that differ from those produced by the simple impulse function. In the other extreme, waves are generated locally or in a storm area whose distance from the observer is not much different from the dimensions of the radar scattering patch; this is somewhat analogous to being in the near field of an antenna. We take as an example the situation existing at a recent coastal HF radar experiment at Pescadero, California [*Lipa et al.*, 1980], where the dominant ocean waves were generated in a storm zone with the approximate dimensions 650 km × 740 km, with the storm center about 1250 km from the radar. These waves had an rms wave height of 113 cm and a frequency spread of about 0.02 Hz about a centroid frequency of 0.07 Hz. For this situation, finite width models are inadequate and full inversion of the integral equation is called for.

2. THE RADAR CROSS SECTION

We consider narrow beam radar systems with vertical polarization directed at or near grazing incidence. Vertical polarization is the only case of importance because (1) ground or surface wave radars require vertical polarization to attain reasonable propagation distances and (2) the horizontally polarized component of scatter from the sea is several orders of magnitude lower than the vertical component, so that even sky wave radars effectively discriminate only the vertical mode for sea echo. *Barrick* [1972] gives the following relation for the first-order average radar cross section per unit surface area at a Doppler shift ω from the carrier:

$$\sigma^{(1)}(\omega) = 2^6 \pi k_0^4 \sum_{m=\pm 1} S(-2m\bar{k}_0)\delta(\omega - m\omega_B) \quad (1)$$

where $\bar{k}_0$ is the radar wave vector of magnitude k_0, S is the directional ocean wave spectrum, and ω_B is the first-order Bragg frequency given by

$$\omega_B = (2gk_0)^{1/2} \quad (2)$$

with g the gravitational acceleration. The first-order spectrum described by (1) consists of two impulse functions symmetrically placed about the carrier frequency at positions defined by the deep water dispersion equation and with amplitudes proportional to the directional ocean wave spectrum at the Bragg wave vectors $\pm 2\bar{k}_0$, as is shown in Figure 1. In practice, the first-order lines are displaced from their ideal positions because of underlying ocean currents and spread over a finite frequency band by current turbulence and system effects.

The second-order radar cross section and the directional ocean wave spectrum are related by a nonlinear integral equation given by *Barrick* [1972]. We express this equation in the following form:

$$\sigma^{(2)}(\omega) = 2^6 \pi k_0^4 \sum_{m,m'=\pm 1} \int_0^\infty \int_{-\pi}^{\pi} |\Gamma|^2 \delta(\omega - m(gk)^{1/2} - m'(gk')^{1/2}) S(m\bar{k}) S(m'\bar{k}') k dk d\theta \quad (3)$$

where the vectors $\bar{k}$ and $\bar{k}'$ obey the relation

$$\bar{k} + \bar{k}' = -2\bar{k}_0 \quad (4)$$

The quantity Γ is a coupling coefficient that includes the effects of both hydrodynamic and electromagnetic nonlinearities carried to second order in a perturbation theory:

$$\Gamma_{m,m'} = \frac{1}{2}\left[\frac{(\bar{k}\cdot\bar{k}_0)(\bar{k}'\cdot\bar{k}_0)/k_0^2 - 2\bar{k}\cdot\bar{k}'}{(\bar{k}\cdot\bar{k}')^{1/2} + k_0\Delta}\right] - \frac{i}{2}\left[k + k' - \frac{(kk' - \bar{k}\cdot\bar{k}')}{mm'(kk')^{1/2}}\left(\frac{\omega^2 + \omega_B^2}{\omega^2 - \omega_B^2}\right)\right] \quad (5)$$

Barrick and Snider [1977] have shown that the sea echo voltage spectrum after N sample averaging is χ square distributed with N degrees of freedom. They also show that Doppler spectra (both first and second order) become uncorrelated for time intervals greater than approximately 25 s for radar frequencies greater than 10 MHz and that Doppler spectra from different range cells are statistically independent to spatial separations as small as 3 km. These experimental results may be used to optimize the amount of incoherent averaging. In practice, at least 10 and normally more than 100 spectra are incoherently averaged before analysis.

The first-order echo is used to linearize the integral equation in an approximation valid at upper HF for higher sea states (e.g., at 25 MHz for rms ocean wave heights greater than 0.4 m). For small values of k/k_0 it follows from (4) that the vector $\tilde{k}'$ is approximately equal to the Bragg wave vector. The second ocean spectral factor in the integral equation (3) may therefore be removed by normalizing the second-order spectrum by the power in the neighboring first-order peak. This normalization scheme, proposed and implemented by *Barrick* [1977*a*], linearizes the integral and removes unknown system gains and path losses from the data.

Because of previously discussed frequency smearing we integrate the second-order spectrum over a finite frequency window δ. The energy in the first-order line is obtained by integrating over a frequency window of width δ_h, which can conveniently be taken as the width between the half-power points. We then define the following experimental parameters:

$$r_{m,m'}(\omega) = \frac{\int_{\omega-\delta/2}^{\omega+\delta/2} \sigma^{(2)}(\eta)\, d\eta}{\int_{m\omega_B-\delta_h/2}^{m\omega_B+\delta_h/2} \sigma^{(1)}(\eta)\, d\eta} \tag{6}$$

Lowercase R's are used throughout to denote measured quantities, while uppercase are theoretical; script R's denote total energy in the peak, while block R's denote the actual peak function itself.

When we employ models to describe the swell (as in the first two cases considered below), δ is the width of the second-order swell peak. In this case we have integrated out the frequency and are concerned only with the energy in the Doppler peaks; for this case we redefine $r_{m,m'}(\omega)$ in (6) above as $\mathcal{r}_{m,m'}$. When we do a complete inversion of the integral, however (as in the third case below), $\delta = \delta_h$ because the first-order peak width determines the ultimate frequency resolution attainable in the inversion process. Substituting expressions (1) and (3) for the first-order and second-order radar cross sections into (6) gives the approximate linear integral equation:

$$R_{m,m'}(\omega) = \int_{\omega-\delta/2}^{\omega+\delta/2} \int_0^{\infty} \int_{-\pi}^{\pi} |\Gamma_{m,m'}|^2 \delta(\eta - m(gk)^{1/2} - m'(gk')^{1/2}) S(m\tilde{k})\, k\, d\theta\, dk\, d\eta \tag{7a}$$

In the absence of frequency smearing, we define the quantity

$$R'_{m,m'}(\omega) = \lim_{\delta\to 0} \frac{R_{m,m'}}{\delta} = \int_0^{\infty} \int_{-\pi}^{\pi} |\Gamma_{m,m'}|^2 \delta(\omega - m(gk)^{1/2} - m'(gk')^{1/2}) S(m\tilde{k})\, k\, d\theta\, dk \tag{7b}$$

which is just the second-order radar cross section normalized by the first-order energy.

The second-order sea echo appears as four side bands surrounding the two first-order Bragg lines (see Figure 1), representing the four combinations of m, $m' = \pm 1$. In contrast with previous impressions in the literature, the coupling coefficient $|\Gamma_{m,m'}|^2$ varies significantly with direction. If this were not so, it would be easy to show that the four side bands defined by (7) would all have the same amplitudes and shapes, making it difficult to extract many swell parameters. More relevant details about the coupling coefficient are found in the appendix.

In the next section we show how to invert (7) to give the ocean wave directional spectrum. The standard error in the derived parameters depends on the data covariance matrix. To derive this, we note that $R_{m,m'}$ is defined in (6) as the ratio of sums of χ^2 power spectral samples and is therefore itself a random variable that follows an F distribution [*Barrick*, 1980]. If the numerator and denominator are sums of M and N independent samples, respectively, in the limit of large N, the F distribution becomes χ^2 with an effective number of degrees of freedom L_e given by

$$1/L_e = 1/M + 1/N \tag{8}$$

Barrick and Lipa [1979*b*] show theoretically that power spectral values at different Doppler frequencies are statistically independent. The covariance matrix of a set of ratios $R_{i,i'}$ is therefore diagonal with elements given by

$$\langle \Delta\mathscr{R}_{i,i'} \Delta\mathscr{R}_{j,j'} \rangle = \frac{\mathscr{R}^2_{i,i'}}{L_e} \delta_{ii'} \delta_{jj'} \tag{9}$$

3. INTERPRETATION FOR OCEAN WAVE PARAMETERS

3.1. *Swell of a single wavelength and direction*

We write the total wave height spectrum at a wave vector $\bar{k}$ as the sum of a continuous high-frequency wind wave spectrum $S_w(\bar{k})$ and a swell component generated at great distance that is an impulse function in wave vector space:

$$S(\bar{k}) = S_w(\bar{k}) + H_s^2 \delta(\bar{k} - \bar{k}_s) \tag{10}$$

where H_s is the rms wave height of the swell and $\bar{k}_s$ is the swell wave vector that has magnitude k_s and propagation angle θ_s with respect to the radar beam (i.e., away from the radar). When this spectrum is substituted into the integral equation (7*a*), the right-hand side separates into a continuous wind wave spectrum, with cross-spectral terms due to the interaction of swell and wind waves given by

$$R_{m,m'}(\omega) = H_s^2 \int_{\omega-\delta/2}^{\omega+\delta/2} \int_0^\infty \int_0^{2\pi} |\Gamma_{m,m'}|^2 \delta(\eta - m(gk)^{1/2} - m'(gk')^{1/2}) \delta(m\bar{k} - \bar{k}_s) k dk d\theta d\eta \tag{11}$$

and terms due to the swell interacting with swell. The latter terms can be seen to be a very resonant phenomenon that can only be observed at a single radar operating frequency that occurs at lower MF, well below our range of consideration here. The first set of terms representing wind wave/wind wave interactions involves only short-period waves and occurs at Doppler frequencies further removed from the Bragg lines than the swell peaks (see Figure 1) and thus lies outside our range of consideration; their inversion is treated elsewhere [*Barrick and Lipa,* 1979*a, b*]. It is the cross-spectral terms represented by (11) that contain the information on the swell. In (11) the wind wave spectrum has been removed by the normalization defined in (6).

The integration in (11) may be performed immediately by using the delta function constraints on the integration variables. Four sharp spikes occur in the Doppler spectrum with frequencies and powers given by

$$\omega_{m,m'} = m\omega_s + m' [\omega_B^4 + 2m\omega_s^2 \omega_B^2 \cos\theta_s + \omega_s^4]^{1/4} \tag{12}$$

where

$$\omega_s \equiv (gk_s)^{1/2} \qquad \omega_B \equiv (2gk_0)^{1/2}$$

$$\mathscr{R}_{m,m'} = 2H_s^2 |\Gamma_{m,m'}|^2 \tag{13}$$

where $\Gamma_{m,m'}$ is evaluated at $\bar{k}_s$ and $\bar{k}'$ obtained from (4). For typical HF radar frequencies, $k_s \ll k_0$, and the above equations show that the swell peak frequencies are close to the Bragg frequency, often occurring in the null between the first-order line and the peak of the wind wave spectrum (see Figure 1). We define $\Delta\omega^+$ as the radian frequency displacement between the two swell peaks surrounding the approaching Bragg line; likewise for $\Delta\omega^-$ with respect to the two swell peaks surrounding the receding Bragg line. Estimates of swell spatial wave number and direction may be made from the peak frequencies (12) through the equations

$$k_s = \left(\frac{1}{16g}\right)(\Delta\omega^+ + \Delta\omega^-)^2 \tag{14}$$

$$\theta_s = \cos^{-1}\left(8\omega_B \frac{(\Delta\omega^+ - \Delta\omega^-)}{(\Delta\omega^+ + \Delta\omega^-)^2}\right) \tag{15}$$

The values of $\omega_{m,m'}$ are calculated by finding the centroid frequency of the spectral peak between the half-power points. *Barrick* [1980] has calculated a general expression for the standard deviation of a centroid frequency for a spectrum that has χ^2 statistics. This expression is insensitive to the exact shape of the peak; if we therefore assume a Gaussian form for convenience, he shows that the standard deviation of the frequency estimate is

$$Sd(\omega) = \frac{\Delta}{2}\left(\frac{N}{K}\right)^{1/2} \tag{16}$$

where N is the number of samples contained within the half-power width, K is the number of independent spectra used in the sample average, and Δ is the angular frequency spacing between adjacent spectral points. The corresponding errors in the estimates (14) and (15) for k_s and θ_s follow from linear error propagation theory [*Brandt,* 1970]

$$Sd(k_s) = \frac{\Delta}{2}\left(\frac{k_s N}{gK}\right)^{1/2} \tag{17}$$

and

$$Sd(\theta_s) = 8\omega_B \Delta \left(\frac{N}{K}\right)^{1/2} \cdot \left| \frac{[5(\Delta\omega^+)^2 - 6\Delta\omega^+\Delta\omega^- + 5(\Delta\omega^-)^2]^{1/2}}{\sin\theta_s(\Delta\omega^+ + \Delta\omega^-)^3} \right| \sin\theta_s \neq 0 \tag{18}$$

The uncertainty in the estimate of wave number is generally small; that in angle can be large because of the differencing of small frequency shifts in (15).

In an independent analysis based on the amplitudes of the swell peaks, expressed theoretically in (13), we use the maximum likelihood method [*Brandt*, 1970] to give estimates of swell wave height and separate independent estimates of the angle. The following expression is minimized with respect to θ_s and H_s:

$$I(\theta_s, H_s) = \sum_{m,m'} \frac{(r_{m,m'} - \mathscr{R}_{m,m'})^2}{\langle \Delta\mathscr{R}^2_{m,m'} \rangle} \tag{19}$$

where $r_{m,m'}$ are the measured values of the energy in the four Doppler peaks, defined by (6), and where the variance of $\mathscr{R}_{m,m'}$ is defined by (9). Thus we minimize the sum of the weighted squared deviations of the experimental values of $r_{m,m'}$ (including random fluctuations) from the ideal functional form to give the optimum values $\tilde{\theta}_s$ and $\tilde{H}_s$. The residual $I(\tilde{\theta}_s, \tilde{H}_s)$ obeys an approximate χ^2 distribution, and we use a χ^2 test on the validity of the ocean wave spectral model, (10). If the value of $I(\tilde{\theta}_s, \tilde{H}_s)$ is too large, the assumption of this model must be reconsidered and more general models used. These models are considered later in this section.

To obtain the standard deviations in the derived parameters, we expand (13) in a Taylor series about $\tilde{\theta}_s$, $\tilde{H}_s$ to give the approximate expression for the variation in the residual with distance from the optimum in the absence of noise:

$$\Delta\mathscr{R}_{m,m'} = 4H_s|\Gamma_{m,m'}|^2\delta H_s + 2H_s^2 \frac{\partial(|\Gamma_{m,m'}|^2)}{\partial\theta_s}\delta\theta_s \tag{20}$$

which may be expressed in the matrix form

$$\Delta\mathscr{R} = M\Delta\xi \tag{21}$$

where

$$\Delta\mathscr{R} = \begin{bmatrix} \Delta\mathscr{R}_{1,1} \\ \Delta\mathscr{R}_{1,-1} \\ \Delta\mathscr{R}_{-1,1} \\ \Delta\mathscr{R}_{-1,-1} \end{bmatrix} \qquad \Delta\xi = \begin{bmatrix} \delta H_s \\ \delta\theta_s \end{bmatrix}$$

$$M = \begin{bmatrix} 4H_s|\Gamma_{1,1}|^2 & 2H_s^2\dfrac{\partial(|\Gamma_{1,1}|^2)}{\partial\theta_s} \\ \vdots & \vdots \\ 4H_s|\Gamma_{-1,-1}|^2 & 2H_s^2\dfrac{\partial(|\Gamma_{-1,-1}|^2)}{\partial\theta_s} \end{bmatrix}$$

Brandt [1970] shows that when the elements of $\Delta\xi$ are determined by the maximum likelihood method of minimizing expression (19), the covariance matrix C_ξ follows from the covariance matrix C_R defined in (9) through the equation

$$C_\xi = (M^T c_R^{-1} M)^{-1} \tag{22}$$

and the standard deviations of $\tilde{H}_s$ and $\tilde{\theta}_s$ are the square roots of the diagonal elements.

3.2. *Ocean waves with finite beam width and narrow frequency spread*

We now consider a model in which the long-period waves are assumed to have a finite but narrow Gaussian spread σ_k in wave number and to be spread in angle according to a cardioid function of power s about a mean direction. These ocean waves could be generated either at a distance, in which case they would be termed swell, or locally by the wind field or by nonlinear interactions. We retain the subscript s for convenience and define the rms height H_s, the mean wave number k_s, and the mean direction θ_s for the following model ocean wave spectrum:

$$S(\bar{k}) = S_w(\bar{k}) + \frac{H_s^2\Gamma(s/2+1)\exp\left[-\dfrac{(k-k_s)^2}{2\sigma_k^2}\right]\cos^s\dfrac{\theta-\theta_s}{2}}{2^{3/2}\pi\sigma_k k\Gamma(s/2+1/2)} \tag{23}$$

where $\Gamma(x)$ is the gamma function of argument x. The second term is the swell spectral model used, and it is normalized so that its integral is equal to the mean square swell wave height; i.e.,

$$\int_0^\infty kdk \int_{-\pi}^{\pi} d\theta S_s(k,\theta) = H_s^2$$

This model could be applicable when the Doppler peaks produced are spread considerably beyond the half-power width of the first-order peak but are still relatively narrow with respect to their frequency shift from this first-order echo. This could also be discovered because the large residual given by (19) indicates that the double impulse function model is not providing a good fit to the data.

The half-power wave number width k_H and the half-power angular spread θ_H of this model are simply related to the parameters σ_k and s by

$$k_H = 2(2 \ln 2)^{1/2}\sigma_k \qquad \theta_H = 4 \cos^{-1}[(1/2)^{1/s}] \tag{24}$$

Often the nondirectional wave height spectrum is measured with a buoy from a time series of the wave height. In this case a temporal spectrum is obtained rather than a spatial spectrum (i.e., versus ω rather than k). For a narrow band spectral peak the half-power widths of the two are related by means of the gravity wave dispersion equation as

$$\omega_H \simeq \frac{gk_H}{2\omega_s} = \frac{(2 \ln 2)^{1/2} g\sigma_k}{\omega_s} \tag{25}$$

where $\omega_s \equiv (gk_s)^{1/2}$.

Upon substituting (23) into (7b) we derive a closed-form solution for the swell echo Doppler peaks by eliminating the double integral as follows: (1) we employ the delta function constraint along with the relevant Jacobian to eliminate one of the integrals; (2) we employ asymptotic techniques (i.e., the saddle point approximation) to perform the remaining integration. The approximation involved in the second step produces the following result, which is no more than 5% in error under the following assumptions (for ocean waves of period greater than 10 s and radar frequencies greater than 10 MHz): $\omega_H/\omega_s < 0.3$ and $\theta_H < 60°$ ($s > 20$);

$$R'_{m,m'}(\omega) = \frac{2}{\omega_{DH}}\left(\frac{\ln 2}{\pi}\right)^{1/2} \mathscr{R}_{m,m'} \cdot \exp\{-(4 \ln 2)(\omega - \omega_{m,m'})^2/\omega_{DH}^2\} \tag{26}$$

where the peak positions $\omega_{m,m'}$ are identical to those of the impulse function model given by (12). The above expression is normalized so that the integral over ω yields $\mathscr{R}_{m,m'}$; this quantity is given by

$$\mathscr{R}_{m,m'} = \frac{2H_s^2}{A(s)} \int_{-\pi}^{\pi} |\Gamma_{m,m'}(\theta)|^2 \cos^s\left(\frac{\theta - \theta_s}{2}\right) d\theta \tag{27a}$$

where

$$A(s) \equiv \frac{2(\pi)^{1/2}\Gamma(s/2 + 1/2)}{\Gamma(s/2 + 1)} = \int_{-\pi}^{\pi} \cos^s(\phi/2)\, d\phi \tag{27b}$$

The square of the Doppler peak half-power width ω_{DH} is comprised of two terms, one resulting from the finite frequency spread of the wave height spectrum and one produced by its finite angular spread (i.e., $\omega_{DH}^2 = \omega_{DHF}^2 + \omega_{DH\theta}^2$), where

$$\omega_{DHF} = \omega_H \left| m + m' \frac{\omega_s^3 + m\omega_B^2\omega_s \cos\theta_s}{[\omega_B^4 + 2m\omega_B^2\omega_s^2 \cos\theta_s + \omega_s^4]^{3/4}} \right| \tag{28a}$$

$$\omega_{DH\theta} = \frac{\theta_H}{2} \left| \frac{\omega_s^2\omega_B^2 \sin\theta_s}{[\omega_B^4 + 2m\omega_B^2\omega_s^2 \cos\theta_s + \omega_s^4]^{3/4}} \right| \tag{28b}$$

where all ω's are in radians per second and θ_H is in radians. All quantities in these equations have been defined previously.

There are several interesting implications of (26)–(28) that should be noted:

1. The peak centroids or maxima occur at the same positions, $\omega_{m,m'}$, as those for the impulse function model. Hence one can solve for the dominant period (i.e., k_s or ω_s) and direction θ_s by solving (14) and (15) for the spacings between the centroids of the Doppler peaks.

2. The ocean wave frequency spread ω_H does not appreciably affect the energy distributions in the Doppler peaks, as represented by $\mathscr{R}_{m,m'}$ in (27). The wave directional spread, however, does affect this quantity. In the limit of the impulse function in angle ($s \to \infty$), (27a) is seen to reduce identically to (13). In practice, having determined θ_s, ω_s (and knowing ω_B), one would numerically solve the integral (27a) (see the appendix) and then employ maximum likelihood methods discussed in the preceding section to fit equation (27a) to the data in order to determine the rms wave height H_s, independent estimates of direction θ_s, and estimates of the angle spreading parameter s.

3. Of the two contributors to finite Doppler spectral peak width, the one produced by finite ocean wave frequency spread dominates for nearly all practical situations, as is seen by comparing (28a) with (28b). For example, for the wave field at Pescadero described in the introduction, it can be seen that $(\omega_{DHF}/\omega_{DH\theta})^2 > 16$, implying that $\omega_{DH} \simeq \omega_{DHF}$. Hence the width of the echo Doppler peaks, ω_{DH}, can be related directly to the frequency

width spread of the ocean wave spectrum, ω_H, directly through (28*a*).

3.3. *General inversion for swell*

If the radar spectrum close to the first-order lines has a broad distribution, rather than displaying narrow peaks, we use a general inversion method that applies to both swell and wind-generated seas. The ocean wave spectrum is expanded as a finite Fourier series in angle with coefficients that are functions of wave number:

$$S(\bar{k}) = \frac{1}{2\pi} \sum_{i=-n}^{n} c_i(k) tf_i(\theta) \tag{29}$$

where

$$tf_i = \cos(i\theta) \qquad i \geq 0$$

$$tf_i = \sin(i\theta) \qquad i < 0$$

We assume the ocean wave spectrum is constant within N wave number bands $k_j - \delta_j/2$ to $k_j + \delta_j/2$ and substitute (29) into the integral equation (7*a*), which reduces to the following linear form:

$$R_{m,m'}(\omega) = \sum_{i=-n}^{n} \sum_{j=1}^{N} K_{ijmm'}(\omega) c_i(k_j) \tag{30}$$

where the coefficients are given by

$$K_{ijmm'}(\omega) = \frac{1}{2\pi} \int_{\omega-\delta/2}^{\omega+\delta/2} \int_{k_j-\delta_j/2}^{k_j+\delta_j/2} \int_{0}^{2\pi} |\Gamma_{m,m'}|^2 \cdot \delta(\eta - m(gk)^{1/2} - m'(gk')^{1/2}) tf_i(\theta) k\, d\theta\, dk\, d\eta \tag{31}$$

The integral in (31) is performed numerically by using a method developed by *Lipa* [1977]. The values of the coefficients $K_{ijmm'}$ for negative values of i are very small because the coupling coefficient is an even function of angle, and the frequency contours defined by the delta function constraint are almost circular. For $i < 0$, $tf_i(\theta)$ is an odd function of angle, and it follows that the integral in (31) is nearly zero. It is therefore impossible to obtain the corresponding values of c_i for $i < 0$ by inverting (30). This constraint applies to a narrow beam radar with a single look direction; it can be circumvented by using two or more look angles or by use of the rotating broad beam antenna described by *Barrick and Lipa* [1979*b*]. Values of the even Fourier coefficients may be obtained by inverting the linear equations (30) using methods developed by *Phillips* [1962] and *Twomey* [1963] and previously applied to radar sea echo inversion by *Lipa* [1977] and *Barrick and Lipa* [1979*b*]. The number of Fourier coefficients that can be derived with adequate accuracy from a given data set depends on the random fluctuations of the data and the magnification of error that occurs during the inversion process. We have inverted measured data to give the first three even Fourier coefficients $c_0(k)$, $c_1(k)$, and $c_2(k)$ with adequate accuracy [*Lipa et al.*, 1980].

The nondirectional coefficient $c_0(k)$ is merely the ocean wave nondirectional spectrum, since it follows from (29) that $c_0(k)$ is the integral of the directional wave spectrum over angle. The directional coefficients $c_1(k)$ and $c_2(k)$ do not admit to a quick interpretation in terms of important directional parameters such as the dominant or mean wave direction. *Barrick and Lipa* [1979*b*] show how they may be interpreted in terms of the cardioid model for the angular distribution, which gives the dependence at a given wavelength as $\cos^s[(\theta - \theta_s)/2]$, where θ is the wave angle at a selected direction. This model requires that the following relations be obeyed:

$$\frac{c_1(k)}{c_0(k)} = \frac{2s}{(s+2)} \cos\theta_s \qquad \frac{c_2(k)}{c_0(k)} = \frac{2s(s-2)}{(s+2)(s+4)} \cos 2\theta_s \tag{32}$$

Estimates of s and θ_s at each wave number may be determined by fitting these equations to the values of $c_i(k)$ obtained by inversion of the radar spectrum. The angle θ_s can then be interpreted as the mean wave direction. Since only the even coefficients c_0, c_1, and c_2 are derived from the above general inversion process, a unique determination of θ_s and s is not always possible without additional information.

4. CONCLUSIONS

Our analysis reverses the impressions given by prior works on the extraction of sea state parameters from HF radar echoes in that it shows that long-wave directions can be determined from the second-order echo. The reason for this is that the second-order Doppler structure is sensitive to the directional properties of long waves. Inclusion of this dependence in the analysis results in more accurate

estimates of height and period as well as giving the direction itself. A model suitable for narrow band/beam ocean waves allows the direct extraction of the angular beamwidth and frequency bandwidth also. Expressions for the errors in these estimates are derived and presented.

The three techniques presented here—including the two closed-form models we derive—have been successfully tested against measured data from three separate experiments; they have been compared with several alternate sources of 'surface truth' by *Lipa et al.* [1980], whose analysis of the considerable amount of data is extensive and draws heavily upon the models and methods presented here. Our purpose in this paper is to derive and present simple models and methods that have been proven against data, along with a discussion of how and when to use them. We derive error estimate expressions for our results and show specifically how to use maximum likelihood principles for the models employed here. Hence this paper should provide all the tools a user needs to extract long-period ocean wave parameters from narrow beam second-order HF sea echo Doppler spectra.

A couple of limitations should be noted. First, although use of a single narrow beam allows the extraction of a surprising amount of directional information, one is restricted by the right/left ambiguity with respect to the radar beam. Therefore unless one can scan the beam (or employ multiple beams), one is forced to guess or use additional information to remove this ambiguity. Second, for the two models derived, the ocean waves have been assumed to have a single dominant direction, although they may be spread in angle. If two Doppler peaks can be resolved in the data representing different swell frequencies and directions, then each can be handled separately using the models. If, however, wave trains from different directions are sufficiently close in wave frequency that they cannot be separately distinguished in the Doppler records, then these models are likely to give spurious results. Such a situation would be signalled by the χ^2 test applied to the residual, (19), indicating a poor fit of the model. Also, internal inconsistencies would be observed. For example, the directions obtained from peak positions would disagree with those obtained from maximum likelihood analysis of the peak amplitudes. In this case, full inversion of the integral equation using the method described in section 3.3 must be performed.

APPENDIX

To illustrate the strong directional dependence of the coupling coefficient, we show plots of this quantity, $|\Gamma_{m,m'}|^2$, versus θ_s in Figure 2 for a typical example: 13-s swell at both 10 and 20 MHz. These plots are normalized to k_0^2, the radar wave number. Also shown is the $\cos^2 \theta_s$ function (dotted) for comparison. The amplitudes of the four spectral peaks for the impulse function model of swell are directly proportional to this coupling coefficient, from (13). Therefore one can clearly see that these amplitudes will vary greatly, even disappearing when the swell propagates perpendicular to the radar beam.

The reason for the asymmetric front-to-back

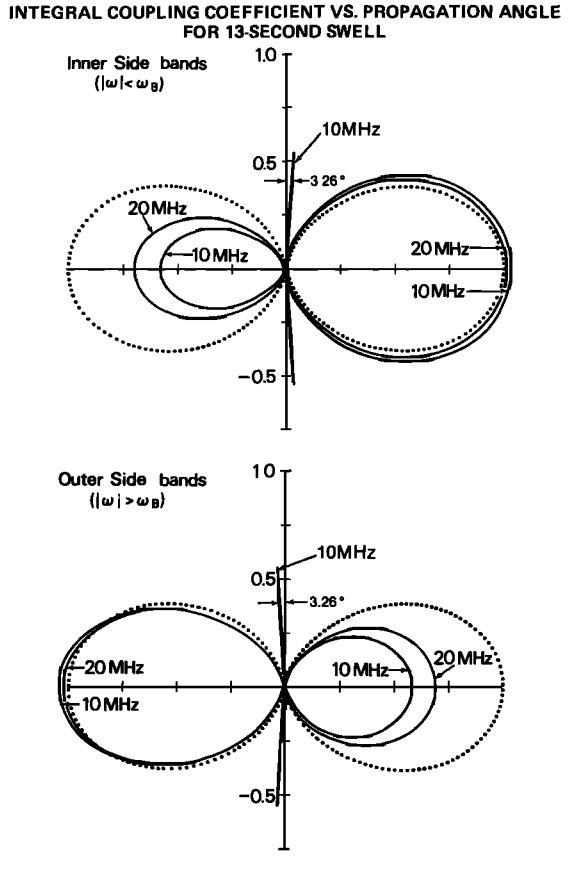

Fig. 2. Polar plots of normalized coupling coefficient (divided by k_0^2), $|\Gamma_{m,m'}|^2$, for 13-s swell at two radar frequencies. Plots are versus θ_s, the angle between the radar look direction and the swell propagation direction. Dotted curves give $\cos^2 \theta_s$ function for comparison. For positive Doppler side bands, θ_s in the above plots is measured from the $+x$ axis; for negative side bands, from the $-x$ axis.

shape lies with the existence of the first term (the electromagnetic interaction effect) of the coupling coefficient, (5). Even though the hydrodynamic interaction term (the second term) is larger, one clearly cannot neglect the electromagnetic term. For if the first term were zero, the coupling coefficient would have the $\cos^2 \theta_s$ form and there would be no front-back asymmetry. In that event the odd directional cosine coefficients c_1, c_3, etc., contained in the wave height spectrum (29) would be indeterminable. In other words, one would not be able to distinguish swell at θ_s from swell at $180° - \theta_s$. As it is, a single narrow beam can extract c_0, c_1, c_2, c_3, and possibly higher odd coefficients if the data are not too noisy.

The other distinct features of these plots are the spikes (shown only for the 10-MHz case); these occur when the two ocean wave trains are perpendicular, i.e., $\bar{k} \cdot \bar{k}' = 0$. In this event the radical $(\bar{k} \cdot \bar{k}')^{1/2}$ occurring in the denominator of the coupling coefficient vanishes, making the coefficient itself very large. This condition of perpendicularity of the wave trains is referred to as the 'corner reflector' condition [*Trizna et al.*, 1977], and it has been suggested that this effect can be a significant contribution to second-order scatter. For long waves the total energy contained in this spike is very small, less than the energy contained within a 1° sector at the pattern maximum; this spike energy is even 4 times less at 20 MHz. Since narrow band swell on the open ocean always spans a sector exceeding 4°, these spikes could never contain enough energy to be seen. Further proof of this is evident from the many cases of long-wave propagation examined by *Lipa et al.* [1980], where four second-order Doppler peaks are always seen; the corner reflector condition would produce only two such peaks. (For example, for swell slightly approaching the radar such that $\bar{k}_s \cdot \hat{x} < 0$, these peaks would be positioned one on the positive side of each Bragg line.)

The regions $\bar{k} \cdot \bar{k}' > 0$ and $\bar{k} \cdot \bar{k}' < 0$, on the other hand, explain the front-to-back asymmetry in the larger lobes of these patterns. The larger lobe of each pattern is produced when $\bar{k} \cdot \bar{k}' > 0$, resulting in the square root of this quantity being real. This physically means that the intermediate electromagnetic wave interacting with the two ocean waves of wave vectors $\bar{k}$ and $\bar{k}'$ (one of which is the swell wave vector) is 'propagating,' and the electromagnetic and hydrodynamic terms are then seen to add in quadrature. With the smaller lobe, however, the argument of the radical is negative, and hence the radical is imaginary, i.e., $(\bar{k} \cdot \bar{k}')^{1/2} = (-|\bar{k} \cdot \bar{k}'|)^{1/2} = i(|\bar{k} \cdot \bar{k}'|)^{1/2}$. In this case the intermediate electromagnetic wave is not propagating but is 'evanescent'; then the electromagnetic and hydrodynamic terms are no longer in quadrature but are in phase and subtracting. In the former case an approximate factor for the coupling coefficient at the larger lobe maximum is $1 + (\omega_s/\omega_B)^2$, while in the latter case the appropriate factor at the smaller lobe maximum is $[1 - (\omega_s/\omega_B)]^2$.

Looking at Figure 2, it is tempting to suggest that the upper and lower plots are identical if they are flipped around. One might go further and say that the coupling coefficient can be modeled accurately by a $\cos^2 \theta_s$ pattern whose amplitude factor in one direction is $[1 + (\omega_s/\omega_B)^2]$ and in the other is $[1 - (\omega_s/\omega_B)]^2$; this would result in a closed-form solution to (27). However, this simplification would produce identical sets of Doppler peaks surrounding each of the two first-order Bragg peaks, and this has been observed in measured data not to be the case for $|\cos \theta_s| < 0.5$ [*Lipa et al.*, 1980]. Closer examination of the coupling coefficient, as plotted in Figure 2, shows that, for example, at $|\cos \theta_s| = 0.5$ (i.e., $\theta_s = 60°$ and 120°) the values of the smaller lobes differ as much as 25% from each other. This is sufficient to produce significant error in the swell parameter extraction process. Therefore one should employ the exact expression for the coupling coefficient in (13) and (27) and in the full integral inversion process. The coupling coefficient can be calculated quickly on the computer, and this should be done rather than attempting to use any 'approximation' to the exact coupling coefficient.

Acknowledgment. Support by the National Oceanic and Atmospheric Administration under contract 03-78-B01-119 is gratefully acknowledged.

REFERENCES

Barrick, D. E. (1971), Dependence of second-order sidebands in HF sea echo upon sea state, in *IEEE G-AP International Symposium Digest*, pp. 194–197, Institute of Electrical and Electronics Engineers, New York.

Barrick, D. E. (1972), Remote sensing of sea state by radar, in *Remote Sensing of the Troposphere*, edited by V. E. Derr, U.S. Government Printing Office, Washington, D. C.

Barrick, D. E. (1977*a*), The ocean waveheight nondirectional spectrum from inversion of the HF sea-echo Doppler spec-

trum, *Remote Sensing Environ., 6,* 201–227.

Barrick, D. E. (1977*b*), Extraction of wave parameters from measured HF sea echo Doppler spectra, *Radio Sci., 12,* 415–424.

Barrick, D. E. (1980), Accuracy of parameter extraction from sample-averaged sea-echo Doppler spectra, *IEEE Trans. Antennas Propagat., AP-28,* 1–11.

Barrick, D. E., and B. J. Lipa (1979*a*), Ocean surface features observed by HF coastal ground-wave radars: A progress review, in *Ocean Wave Climate,* edited by M. D. Earle and A. Malahoff, pp. 129–152, Plenum, New York.

Barrick, D. E., and B. J. Lipa (1979*b*), A compact transportable HF radar system for directional coastal wavefield measurements, in *Ocean Wave Climate,* edited by M. D. Earle and A. Malahoff, pp. 153–201, Plenum, New York.

Barrick, D. E. and J. B. Snider (1977), The statistics of HF sea-echo Doppler spectra, *IEEE Trans. Antennas Propagat., AP-25,* 19–28.

Brandt, S. (1970), *Statistical and Computational Methods in Data Analysis,* North-Holland, Amsterdam.

Crombie, D. D. (1955), Doppler spectrum of sea echo at 13.56 Mc/s, *Nature, 175,* 681–682.

Hasselmann, K. (1971), Determination of ocean wave spectra from Doppler radio return from the sea surface, *Nature, 229,* 16–17.

Hasselmann, K., D. B. Ross, P. Müller, and W. Sell (1976), A parametric wave prediction model, *J. Phys. Oceanogr., 6,* 200–228.

Kinsman, B. (1965), *Wind Waves,* p. 67, Prentice-Hall, Englewood Cliffs, N. J.

Lipa, B. J. (1977), Derivation of directional ocean wave spectra by integral inversion of second-order radar echoes, *Radio Sci., 12,* 425–436.

Lipa, B. J. (1978), Inversion of second-order radar echoes from the sea, *J. Geophys. Res., 83,* 959–962.

Lipa, B. J., D. E. Barrick, and J. W. Maresca, Jr. (1980), HF radar measurements of long ocean waves, submitted to *J. Geophys. Res.*

Long, A. E., and D. B. Trizna (1973), Mapping of North Atlantic winds by HF radar sea backscatter interpretation, *IEEE Trans. Antennas Propagat., AP-21,* 680–685.

Maresca, J. W., Jr., and T. M. Georges (1980), Measuring rms wave height and the scalar ocean wave spectrum with HF skywave radar, *J. Geophys. Res., 85,* 2759–2971.

Phillips, D. L. (1962), A technique for the numerical solution of certain integral equations of the first kind, *J. Ass. Comput. Mach., 9,* 84–97.

Stewart, R. H., and J. R. Barnum (1975), Radio measurements of oceanic winds at long ranges: An evaluation, *Radio Sci., 10,* 853–857.

Trizna, D. B., J. C. Moore, J. M. Headrick, and R. W. Bogle (1977), Directional sea spectrum determination using HF Doppler radar techniques, *IEEE Trans. Antennas Propagat., AP-25,* 4–11.

Twomey, S. (1963), On the numerical solution of Fredholm integral equations of the first kind by inversion of the linear system produced by quadrature, *J. Ass. Comput. Mach., 10,* 97–101.

Wait, J. R. (1966), Theory of HF ground wave backscatter from sea waves, *J. Geophys. Res., 71,* 4839–4842.